NUCL SCI TECH (2020) 31:4
https://doi.org/10.1007/s41365-019-0710-3

Adsorption behaviour of Eu(III) on natural bamboo fibres: effects of pH, humic acid, contact time, and temperature

Tao Yu[1,2] · Jun Yang[2] · Ze-Yang Wang[2]

Received: 6 March 2019 / Revised: 21 May 2019 / Accepted: 26 May 2019 / Published online: 19 December 2019

Abstract To study the adsorption properties of organic functional groups in plant fibres and identify a highly efficient and affordable adsorbent for radioactive wastewater treatment, natural bamboo fibre (NBF) samples were prepared, and the adsorption properties of Eu(III) on NBFs were studied under given experimental conditions. The effects of the pH, solid-to-liquid ratio, background ions, humic acid, contact time, and temperature on the adsorption behaviour of Eu(III) on NBFs were investigated. Adsorption was greatly influenced by pH, and the adsorption curves presented two inflection points at pH $\approx$ 7 and pH $\approx$ 11. Moreover, while the ionic strength presented a negative effect at pH $<$ 7, the high ionic strength favoured adsorption at pH $>$ 7. During adsorption on NBFs, the –OH, C–H, O–H, C–O, and C=O were the main adsorption groups. Hydrolysis occurring on the NBF surface caused the adsorption process to become increasingly difficult at pH $>$ 7. The maximum adsorption capacity of NBFs was 147.6 mg/g at 308 K, and the adsorption could be described using the pseudo-second-order kinetic model. The adsorption of Eu(III) on NBFs was a spontaneous and endothermic process according to the thermodynamic parameters of the process, and the adsorption thermodynamics could be well described using the Freundlich adsorption model. Therefore, NBFs were determined to be an efficient, inexpensive, and easily disposable sewage treatment material.

Keywords Adsorption · Eu(III) · Natural bamboo fibre · Organic functional group

1 Introduction

As nuclear science continues to develop, researchers have been focusing on the adsorption and migration of radionuclides on natural adsorbents, in particular the treatment and disposal of radioactive waste [1–3]. Eu(III) is a lanthanide rare-earth element that is often used to simulate trivalent actinides owing to its physicochemical properties. Because Eu(III) ions are similar to Am(III), it could be used to substitute it, and thus, mitigate the difficulties in producing Am(III) and its high cost. Eu(III) adsorption on soil, clay minerals, and fibres has been intensively studied, and it was determined that Eu(III) usually reacts with adsorbents via cation exchange or surface complexation [4]. Owing to the developments in adsorption research, an increasing number of adsorbents have been prepared and tested. Nevertheless, these adsorbents tended to be expensive and difficult to scale. According to some theories, the adsorption process could be divided into four steps: bulk transport, film diffusion, intraparticle diffusion, and adsorption, where the second and third steps are the control steps [5]. At present, researchers are focusing on four types of adsorbent materials: inorganic materials, organic polymers, carbon family

This study was supported by the National Natural Science Foundation of China (No. 21561001) and the Natural Science Foundation of Jiangxi Province, China (No. 20161BAB203100).

✉ Tao Yu
tyu@ecit.edu.cn

[1] Engineering Research Center of Nuclear Technology Application (East China University of Technology), Ministry of Education, Nanchang 330013, China

[2] School of Nuclear Science and Engineering, East China University of Technology, Nanchang 330013, China

materials, and porous framework materials. Among them, cellulose is considered to be the first most abundant polymer in nature that can also be used as potential adsorbent owing to its nontoxicity, affordability, and easy functionalisation [6]. Moreover, novel nanomaterials and magnetic materials have been prepared and the adsorption mechanism of heavy metals on them has been analysed using batch techniques, spectral analysis, surface complexation models, and theoretical calculations [7, 8].

China is rich in plant fibre resources, and plant fibres are widely used to treat environmental pollution and agricultural waste, according to previously published papers [9, 10]. Moreover, China is rich in bamboo and wood fibre resources and is the largest producer of bamboo fibre in the world. Bamboo fibre is a green, renewable, and biodegradable fibrous material [11, 12]. In addition to natural bamboo fibre (NBF), other biological materials such as natural or modified chitosan, cellulose, and microorganisms are used for the adsorption or removal of nuclides. These materials possess many organic functional groups, such as –CH, –OH, and –C=O, and exhibit satisfactory adsorption properties for radionuclides [13], thus resulting in good application prospects for treating radioactive waste and preventing nuclear pollution [14, 15].

As lanthanide rare-earth element, Eu(III) is often used to simulate trivalent actinides owing to its physicochemical properties. Consequently, Eu(III) adsorption on soil, clay minerals, and fibres has been studied intensively [4, 16].

2 Experimental

2.1 Instruments and reagents

An X-650 (Hitachi) scanning electron microscope, an IRPrestige-21 (Shimadzu) Fourier-transform infrared (FT-IR) spectrometer, and a 721E (INESA Analytical Instrument Co., Ltd) visible spectrophotometer were used in this study.

The Eu(III) standard solution comprising Eu_2O_3 was supplied by Ganzhou Deshipu Advanced Material Resource Co., Ltd. Accurately weighed 0.40 g Eu_2O_3 was dissolved in 1.0 mol/L HCl solution and was then transferred into a volumetric flask and diluted with distilled water to 1000 mL. The concentration of obtained Eu(III) solution was 2.273×10^{-3} mol/L.

Arsenazo III (1.0 g/L aqueous solution), pH 2.8 acetic acid–sodium acetate solution, and 0.1% (v/v) ascorbic acid aqueous solution were used as colour developer, buffer, and masking agent, respectively. Distilled water was used for all experiments.

2.2 Preparation of NBF samples

The joint and crust were removed from a piece of fresh bamboo stem (which was grown for more than 3 years), and the stem was cut into 10-cm-long and 2-cm-wide pieces. Then, the samples were dried at 150 °C for 1 h and ground in a mortar, thus producing rough NBFs. The NBFs were then soaked in 60 °C water for 24 h, then dried and rolled before removing the impurities. Afterwards, the samples were boiled (their temperature was increased from 30 to 120 °C) in a pressure cooker at the heating rate of 20 °C/min for 1 h.

Subsequently, the NBF samples were treated with 0.1 mol/L sodium hydroxide (NaOH) solution and were then neutralised with acetic acid. To observe the microfibril structure of the NBF surface, a 10% nitric acid and 10% chromic acid mixed solution (1:1 volume ratio) was used to treat the fibres and remove the hemi-cellulose, lignin, and other non-cellulose elements from the surface of fibres. The procedure was performed at 60 °C for 5 min, and the samples were maintained at 25 °C for 24 h. Then, the samples were washed with distilled water and dried. The obtained NBFs were ground to pass through an 80-mesh sieve (< 0.2 mm) for the standby application.

2.3 Adsorption procedures

The adsorption of Eu(III) on NBFs was assessed at different temperatures: 25, 35, and 50 °C (298, 308, and 323 K, respectively). Certain amounts of NBFs, sodium chloride (NaCl) solution, humic acid (HA) solution, and Eu(III) solution were added to Erlenmeyer flasks. Trace amounts of HCl and NaOH solutions were added to adjust the acidity to the desired pH value. Then, distilled water was added to the flasks to obtain 50 mL mixtures. The mixtures were shaken in an oscillator at a certain temperature for a certain time to reach adsorption–desorption equilibrium, when the concentration of Eu(III) in the solution no longer changed. Then, 10 mL solution was pipetted into a centrifuge tube (15 mL) and was centrifuged at the speed of 5000 r/pm for 10 min. Furthermore, 5.0 mL supernatant was pipetted into a colorimetric tube, and 1.0 mL ascorbic acid, 5.0 mL buffer, and 1.0 mL Arsenazo III solutions were added into the tube. The final volume was set with water, and the concentration of Eu(III) was determined using the spectrophotometric method. Lastly, the quantity of adsorbed radionuclide was calculated by comparing the concentration of Eu(III) before and after the adsorption equilibrium. The adsorption percentage (S, %) and distribution coefficient (K_d) were calculated using the following formulas:

$$S(\%) = \frac{q_e}{c_0} \times \frac{m}{V} \times 100 \quad (1)$$

and

$$K_d = \frac{(c_0 - c_e)}{c_e} \times \frac{V}{m}, \quad (2)$$

where c_0 (mg/L) is the initial concentration of Eu(III) in the liquid phase, c_e (mg/L) is the Eu(III) concentration in the adsorption equilibrium liquid phase, V (L) is the volume of the mixed solution, and m (g) is the mass of NBFs.

3 Results and discussion

3.1 Characterisation of NBF and Eu-NBF

The scanning electron microscopy (SEM) images of NBF and Eu-NBF (after adsorption) are presented in Fig. 1. The results indicate that before adsorption, the NBF surface was very rough and rugged, and many irregular pore- and fibre-like structures were observed on it. The presence of these structures greatly increased the surface area of the NBF, thus allowing for more adsorption sites to be exposed. Moreover, the structure provided important adsorption channels and plenty of adsorption space for the adsorption of metal ions from solution. The pore and filament-like structures of the NBF were favourable for Eu(III) adsorption. After adsorption, the number of pore-like structures of the NBF decreased and the valleys became shallower. This indicated that the number of adsorption sites on the surface decreased.

The energy-dispersive X-ray spectroscopy (EDS) analysis results of the NBF (before adsorption) and Eu-NBF (after adsorption) samples illustrated in Fig. 1 are presented in Fig. 2. The composition of NBF mainly included C, O, and K, and the corresponding element percentages were 26.8%, 71.8%, and 1.2%, respectively (Fig. 2a). Figure 2b depicts the composition of the sample after adsorption, which mainly included C, O, and Eu, and their element percentages were 22.34%, 62.70%, and 14.13%, respectively. Figure 2c–e illustrates the distribution of C, O, and Eu, respectively, on the surface of the Eu-NBF sample (after adsorption) presented in Fig. 1b. Figure 2c–e indicates that the elements and adsorption sites were uniformly distributed on the surface of the sample. These findings indicated that the pore structure and filament-like structure of NBFs conferred them strong adsorption capacity for Eu(III), and K was exchanged with Eu(III) during adsorption.

To study the function of organic functional groups, the FT-IR spectra of the NBF samples were analysed. Figure 3 illustrates the FT-IR spectra of NBF and Eu-NBF samples at pH 4 and 11. The absorption peak at 3313 cm^{-1} was ascribed to the stretching vibration of the –OH radical and was also the characteristic spectral band for all NBF samples; the absorption peaks at 2920 and 2851 cm^{-1} were attributed to the telescopic vibration of $–CH_2–$; the absorption peak at 1634 cm^{-1} belonged to the telescopic vibration of the C=O bond; the absorption peak at 1730 cm^{-1} represented the C=O peak of the –COOH group; the 1634 cm^{-1} absorption peak was allocated to the=C=O group; the absorption peak at 1544 cm^{-1} was generated by the –CONH group; the absorption peak at 1237 cm^{-1} was the characteristic peak of the asymmetric lateral stretching vibration of –C–O–C or wagging vibration of $CH_2(CH_2OH)$; the absorption peak at 1021 cm^{-1} was associated with the –C–O group; and the absorption peak at 601 cm^{-1} was assigned to –C–X (where X is a halogen) [17].

Figure 3 indicates that the spectra of the Eu-NBF sample after adsorption were very similar to the spectra of the

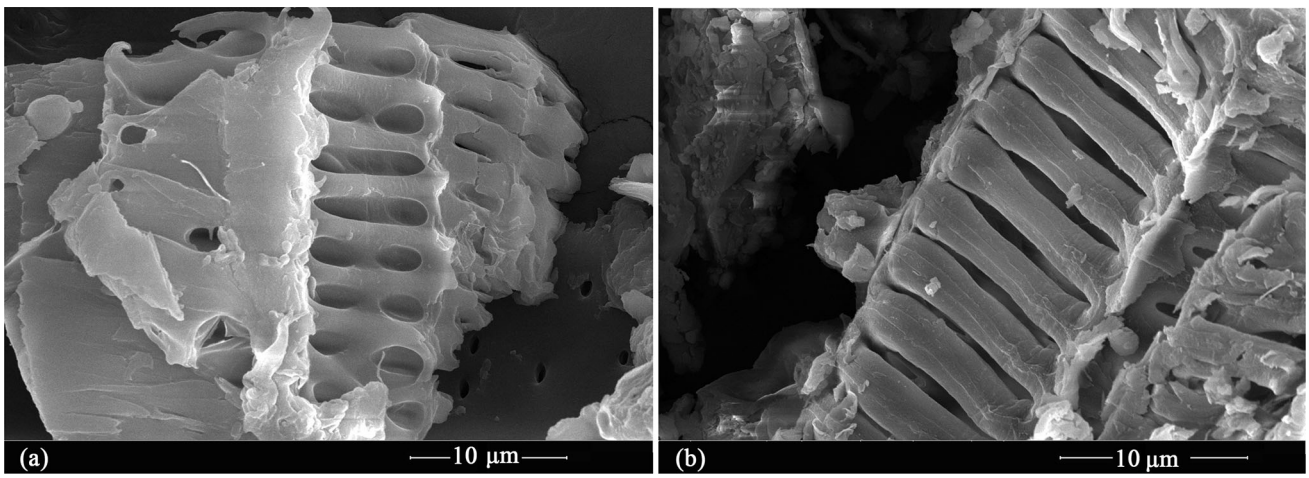

Fig. 1 Scanning electron microscopy images of **a** natural bamboo fibre (NBF) and **b** Eu adsorbed on NBF

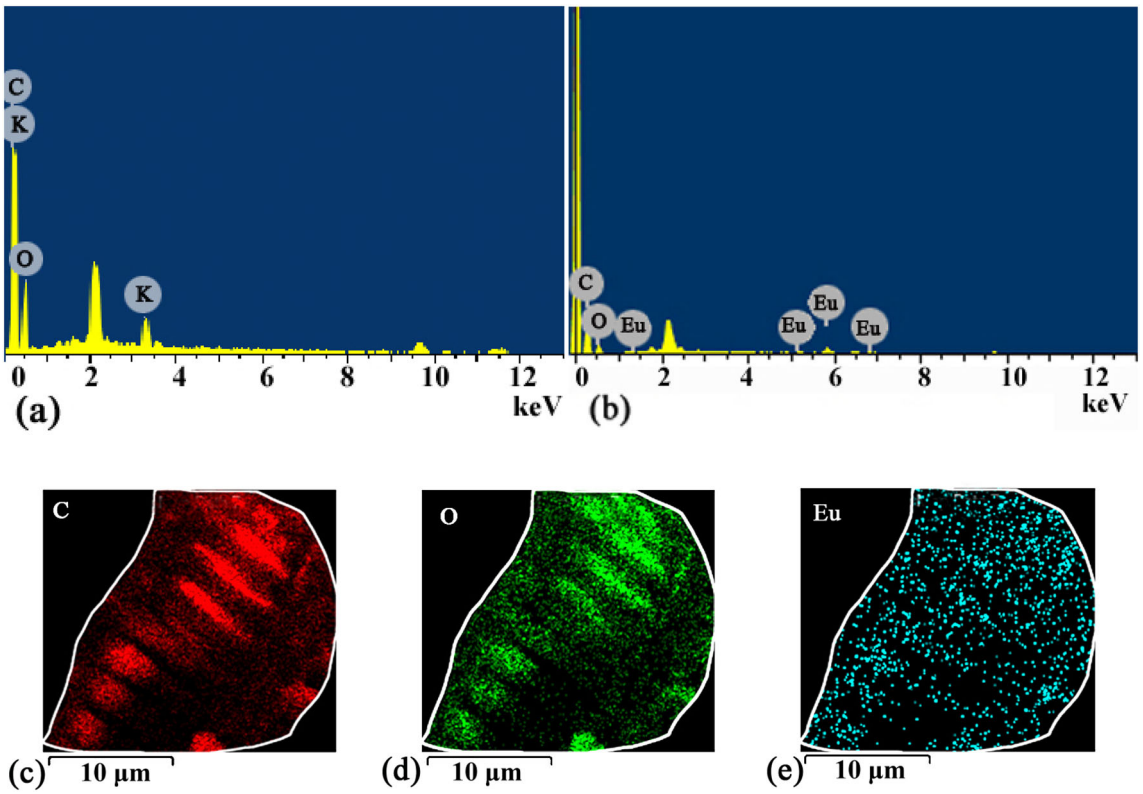

Fig. 2 (Colour online) Energy-dispersive X-ray spectroscopy patterns of **a** natural bamboo fibre (NBF) and **b** Eu adsorbed on NBF (Eu-NBF). Element distribution of **c** C, **d** O, and **e** Eu on surface of Eu-NBF

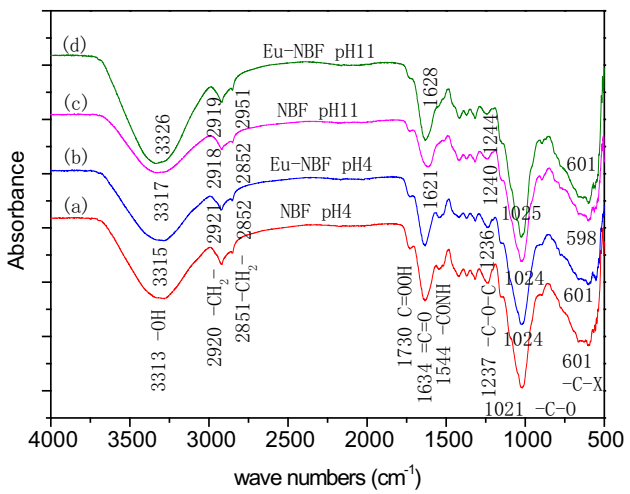

Fig. 3 (Colour online) Fourier-transform infrared spectra of natural bamboo fibre (NBF) and Eu adsorbed on NBF (Eu-NBF): **a** NBF, pH4; **b** Eu-NBF, pH4; **c** NBF, pH11; and **d** Eu-NBF, pH 11

NBF sample (pre-adsorption) at different pH values, and only a couple of peak drifts appeared. These findings indicated that the adsorption process did not destroy the fabric of NBFs. Of all peaks, the skeleton vibration absorption peaks of the hydroxyl –OH, $–CH_2$, C–O, C=O, and polycyclic aromatic hydrocarbons were displaced at 513, 41, 4, 1, and 76 cm^{-1}, respectively, while the positions of the other vibration absorption peaks were essentially unchanged. Therefore, it was concluded that the hydroxyl –OH, C–H, C=O, and C–O were the main adsorption groups of NBFs [18].

At pH 4, the peak of –CONH (1544 cm^{-1}) was present in the spectra of both the NBF and Eu-NBF samples; however, at pH 11 the peak disappeared from their spectra. This indicated that the –CONH group hydrolysed under strong alkaline conditions, which led to the significant change in the adsorption capacity of NBFs.

3.2 Effect of experimental conditions on Eu adsorption

Eu(III) adsorption on NBFs as function of the adsorbent concentration (solid-to-liquid ratio, *m*/*V*) was investigated at pH 6 and 298 K. As the *m*/*V* value of NBFs increased, the adsorption percentage also increased. The experimental error was determined to be less than 5% via repeated experiments at each experimental point. These findings suggested that as the *m*/*V* value increased, the number of adsorption groups on the NBF surface increased and the

total adsorption capacity of the system was improved [19]. The adsorption percentage of Eu(III) decreased to the lowest value (81.2%) at m/V = 0.0428 g/L, while at m/V = 6.0 g/L, the adsorption percentage was the highest (95.8%). To better reflect the influence of other factors on the adsorption process, the adsorption percentage of Eu(III) in subsequent experiments should be not too low or too high. Thus, we selected m/V = 0.6 g/L as the NBF concentration for the following tests.

The effects of the pH and ionic strength on the adsorption process were studied at T = 298 K and m/V = 0.6 g/L. Figure 4 represents the adsorption of Eu(III) on NBFs as function of the pH in the presence of 0, 0.02, 0.04, and 0.1 mol/L NaCl. Eu(III) adsorption was greatly affected by the pH and ionic strength. At pH ≈ 7 and pH ≈ 11, the Eu(III) adsorption curves presented two inflection points at different ionic strengths. At pH < 7 or pH > 11, the adsorption percentage continuously increased as the pH increased, while the adsorption percentage decreased as the pH increased in the pH range of 7–11. While high ionic strength was not conducive for the adsorption process at pH < 7, high ionic strength favoured adsorption at pH > 7. This was because adsorption mainly occurred via cation exchange or outer-sphere complexation at pH < 7 and via inner-sphere complexation at pH > 7. To better reflect the influence of other factors, the following experiments were performed at pH 6.

The effects of different cations (0.02 M LiCl, KCl, and NaCl), anions (0.02 M $NaNO_3$, $NaClO_4$, and Na_2SO_4), and HA on the adsorption of Eu(III) on NBFs were studied under the conditions mentioned above, and the results indicated that Eu(III) adsorption was affected by all these factors. At pH ≈ 7 and pH ≈ 11, the Eu(III) adsorption curve presented turning points in different cations, anions, and HA solutions. The adsorption percentages increased as the pH increased at pH < 7, decreased as the pH increased in the pH range of 7–11, and increased as the pH increased at pH > 11. Moreover, the effects of different ions on the adsorption process could be described as follows: $K^{+-} > Na^+ = Li^+$ and $SO_4^{2-} > ClO_4^- = NO_3^-$ at pH < 7; at pH > 7, the order was reversed. The results also suggested that the presence of HA significantly affected Eu(III) adsorption. At the HA concentrations (c_{HA}) of 0.01 and 0.02 g/L, the presence of HA obviously increased the adsorption of Eu(III) on NBFs in the pH range of 2–12. At pH < 7, the increase in adsorption at c_{HA} = 0.02 g/L was higher than that at c_{HA} = 0.01 g/L, and the opposite trend was observed at pH > 7.

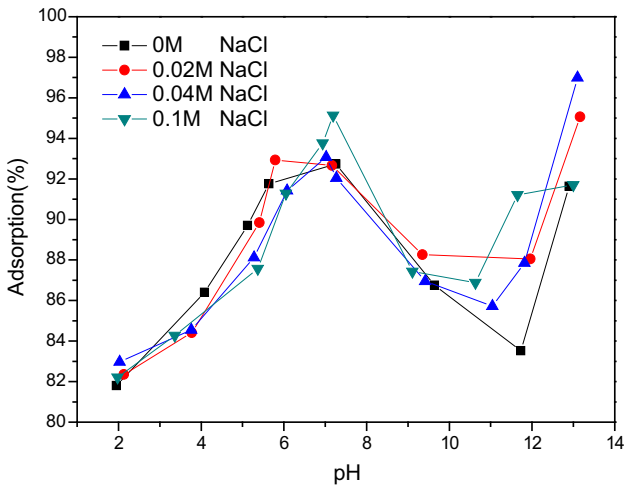

Fig. 4 (Colour online) Adsorption of Eu(III) on natural bamboo fibre (NBF) as function of pH and ionic strength at 298 K and NBF concentration of 0.6 g/L

3.3 Adsorption mechanism

Based on the above characterisation and experimental results, it could be concluded that adsorption occurred via cation exchange or outer-sphere complexation at pH < 7 [Eqs. (3) and (4)] and via inner-sphere complexation or precipitation at pH > 7 [Eqs. (5) and (6)], while $Eu(OH)_3$(aq) weakened the adsorption process in the pH range of 7–13 to a certain extent [Eqs. (7)–(10)]. Here, 'outer-sphere' complexes are the weak or 'second coordination sphere' complexes, while the strong complexes formed between the adsorbate and the adsorbent are usually referred to as 'first coordination sphere' or 'inner-sphere' complexes. These results were attributed to the speciation of Eu(III) in the aqueous solution. The speciation of Eu(III) in solution was analysed, and the main species determined were as follows: Eu^{3+} at pH < 6, $Eu(OH)^{2+}$ and $Eu(OH)_2^+$ at pH 5–9, $Eu(OH)_3$ at pH 7–12, and $Eu(OH)_4^-$ at pH > 11 [20]. From this speciation distribution, it was concluded that the main species of Eu(III) could participate in cation exchange reactions at pH < 7, and the ionic strength negatively affected adsorption in this pH range. In addition, as the pH increased, the adsorption decreased in the pH range of 7–11, and the background ions positively affected the adsorption process. This could be attributed to the speciation of Eu(III) and surface properties of NBFs. Although the hydrolysis of NBFs and appearance of $Eu(OH)^{4-}$ and $Eu(OH)_3$(aq) significantly decreased adsorption, the presence of background ions (e.g., Na^+ and Cl^-) changed the distribution of the Eu(III) speciation and promoted a synergistic effect, which enhanced adsorption under ternary system conditions [21, 22]. Additionally, as the NaCl concentration increased, more Na^+ ions were introduced and became available for possible cation bridging between Eu(III) and the negatively charged functional groups of NBFs. The degree of protonation and point of zero charge decreased as the ionic strength increased, thus facilitating cation adsorption.

Therefore, adsorption was promoted to a certain extent at pH > 7 [22–25].

The experimental results with respect to the effect of pH indicated that at low pH values, the main adsorption mechanism on NBFs was cation exchange or outer-sphere complexation, while at high pH values, the mechanism changed to inner-sphere complexation. The schematic diagrams of the inner- and outer-sphere complexation mechanisms are presented in Fig. 5. Each complexation mechanism involved three conditions, and the outer-sphere complexation was weaker than inner-sphere complexation. These results indicated that surface complexation was greatly affected by the acidity of the solution, and that cation exchange was affected by background ions. According to the characterisation results of NBFs, the NBF surface contained various organic functional groups, such as –OH and –C=O, and these oxhydryls could turn into adsorption sites of variable charge (≡SO–H) which could capture or release protons.

At pH < 7,

$$(\equiv \mathrm{SO})^- + \mathrm{H}^+ \rightleftarrows (\equiv \mathrm{SO{-}H}) \quad (3)$$

and

$$(\equiv \mathrm{SO{-}H}) + \mathrm{Eu}^{3+} \rightleftarrows (\equiv \mathrm{SOEu})^{2+} + \mathrm{H}^+. \quad (4)$$

At pH > 7,

$$(\equiv \mathrm{SO{-}H}) + (\mathrm{EuOH})^{2+} \rightleftarrows (\equiv \mathrm{S{-}OEuOH})^+ + \mathrm{H}^+ \quad (5)$$

and

$$(\equiv \mathrm{SO\text{-}H}) + \left(\mathrm{Eu(OH)_2}\right)^+ \rightleftarrows (\equiv \mathrm{S{-}OEuOH}) + \mathrm{H}^+. \quad (6)$$

Moreover, the hydrolysis process was simulated as follows:

$$(-\mathrm{C=O}) + (\mathrm{H{-}C{-}}) \rightleftarrows (-\mathrm{C{-}C{-}OH}) \quad (7)$$

$$(-\mathrm{C{-}C{-}OH}) \rightleftarrows (-\mathrm{C{-}C{-}O^-}) + \mathrm{H}^+ \quad (8)$$

$$(-\mathrm{CONH}) + \mathrm{H_2O} \rightleftarrows (-\mathrm{COO})^- + \mathrm{H}^+ + (-\mathrm{NH_2}) \quad (9)$$

$$\mathrm{H}^+ + \mathrm{OH}^- \rightleftarrows \mathrm{H_2O} \quad (10)$$

where (–C–H) is the abbreviated structural formula of –C–H_2–, which comprised the basic structure of NBF, and (–C–C–OH) is the speculative product of (–C=O) and (–C–H) under alkaline conditions, which could be protonated and deprotonated. This hydrolysis process rendered the cation exchange and complexation reaction increasingly difficult at pH > 7 and was also the important reason for the decrease in adsorption rate.

The effect of HA on adsorption was also experimentally studied, and the results suggested that the adsorption mechanism of Eu(III) on NBFs could be postulated using the following equations:

$$(\equiv \mathrm{SO{-}H}) + \mathrm{HOOC{-}HA{-}OH} + \mathrm{Eu}^{3+} \rightleftarrows (\equiv \mathrm{S{-}O){-}OC{-}HA{-}O{-}Eu}^{3+} + \mathrm{H_2O} \quad (11)$$

$$(\equiv \mathrm{S{-}O){-}OC{-}HA{-}O{-}Eu}^{3+} + \mathrm{H_2O} \rightleftarrows (\equiv \mathrm{SO{-}H}) + \mathrm{HO{-}HA{-}COOH} + \mathrm{Eu}^{3+} \quad (12)$$

$$(\equiv \mathrm{S{-}O){-}Eu}^{3+} + \mathrm{HO{-}HA{-}COOH} \rightleftarrows (\equiv \mathrm{SO{-}H}) + \mathrm{HO{-}HA{-}COO{-}Eu}^{3+} \quad (13)$$

Here, HA was written as 'HO–HA–COOH' according to its major functional groups. According to the experimental results and above equations, the adsorption strongly depended on pH. Moreover, it was concluded that the –OH and –COOH groups were the main functional groups that affected adsorption. These results suggested that the speciation of Eu(III) was Eu-HA in solution, and Eu-BNF

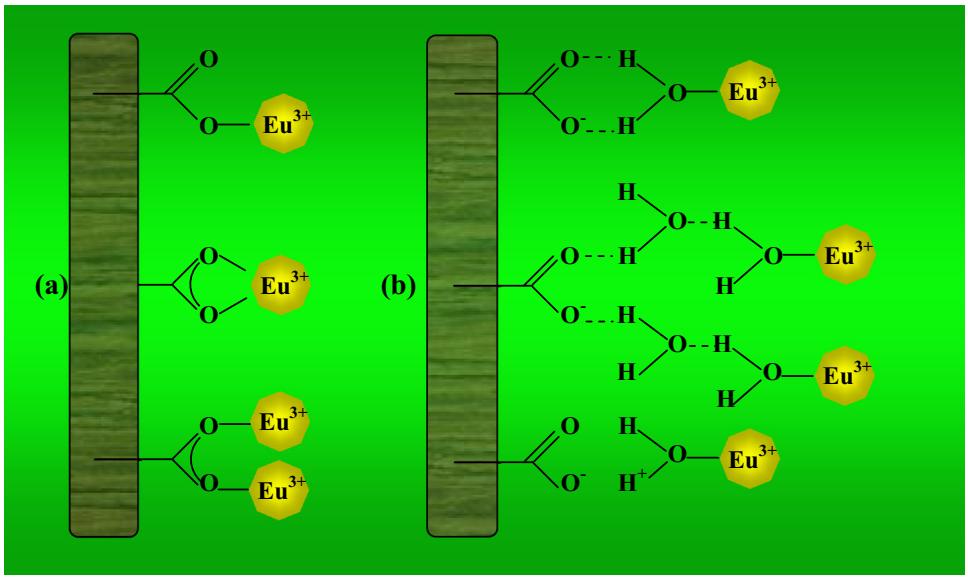

Fig. 5 (Colour online) Schematic diagram of **a** inner- and **b** outer-sphere complexation for Eu(III) adsorption on natural bamboo fibre

(binary complexation), Eu-HA-NBF, or HA-Eu-NBF (ternary complexation) on the NBF surface. These conclusions were consistent with the information previously reported in literature [26, 27].

3.4 Adsorption kinetics

The kinetic study of the adsorption of Eu(III) on NBFs is presented in Fig. 6. Figure 6a displays the effect of the contact time at 298 and 308 K (25 and 35 °C, respectively). The results indicated that the contact time could greatly affect the adsorption process at different temperatures. As the adsorption time increased, the adsorption percentage increased and reached its maximum after 15 h. At 298 and 308 K, the maximum adsorption percentages were 93.4% and 94.1%, respectively. Consequently, the contact time was selected to be 15 h for the following experiments.

To quantitatively analyse the adsorption kinetics of Eu(III) on NBFs, the pseudo-first- and pseudo-second-order kinetic equations were used [Eqs. (14) and (15), respectively] [28, 29]:

$$\ln(q_e - q_t) = \ln q_e - k_1 t, \tag{14}$$

and

$$\frac{t}{q_t} = \frac{1}{k_2 q_e^2} + \frac{1}{q_e} t, \tag{15}$$

where t (h) is the contact time, k_1 (h^{-1}) and k_2 (g/(mg h)) are the pseudo-first- and pseudo-second-order reaction rate constants, respectively, q_t (mg/g) is the adsorption capacity of Eu(III) at time t (h), and q_e (mg/g) is the equilibrium adsorption capacity. These two kinetic models are presented in Fig. 6b, c.

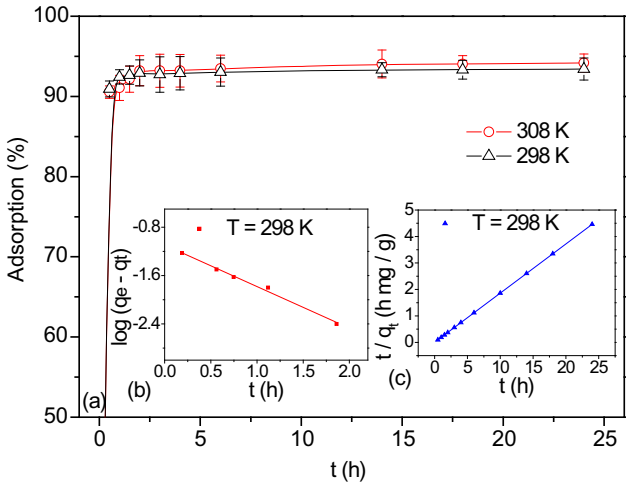

Fig. 6 (Colour online) **a** Adsorption of Eu(III) on natural bamboo fibre (NBF) as function of contact time fitted using the **b** pseudo-first- and **c** pseudo-second-order kinetic models at pH 6.0 and NBF concentration of 0.6 g/L

From Fig. 6b, c, it was determined that the linearity of the experimental data was good at 25 °C. The adsorption parameters were calculated using the slopes and intercepts of the plots generated by graphing the above equations, and the obtained values are given below.

For the pseudo-first-order kinetics equation:

$T = 25\,^{\circ}\mathrm{C}$, $R^2 = 0.990$, $k_1 = 0.689\,h^{-1}$, and $q_e = 0.335\,mg/g$.

For the pseudo-second-order kinetics equation:

$T = 25\,^{\circ}\mathrm{C}$, $R^2 = 0.999$, $k_2 = 7.505\,g/(mg\,h)$, and $q_e = 5.382\,mg/g$.

These results indicated that the pseudo-second-order kinetics model could fit the experimental data better than the pseudo-first-order kinetics one and was more suitable for describing the adsorption of Eu(III). The linear correlation coefficient (R^2) indicated that the pseudo-second-order kinetics model could accurately describe the kinetics of the adsorption reaction because it was very close to 1 [28, 30]. According to the experimental results and data reported in the literature, the adsorption capacity of NBFs for Eu(III) was relatively low, and the time required for the adsorption process to reach equilibrium was relatively long compared with the those of many synthetic or modified materials for other radionuclides (the adsorption capacity is usually higher than 50 mg/g, and the time required for the adsorption process to reach equilibrium is less than 10 h) [6, 31, 32].

The adsorption kinetics of Eu(III) on NBFs could also be described using the diffusion model and Weber–Morris intraparticle diffusion model [33]. The experimental data could be described using the former model as follows:

$$Bt = -\ln(1 - F) - 0.4977, \tag{16}$$

where $B = \pi^2 Di/d^2$, $F = q_t/q_e$, d is the particle radius, and Di is the diffusion coefficient. The latter model could further simulate the diffusion process, and the model equation can be expressed as follows:

$$q_t = K_e t^{0.5} + C, \tag{17}$$

where C is the intercept and K_e (kg/(mg $h^{0.5}$)) is the intraparticle diffusion rate constant. The value of K_e could be calculated from the slope of the linear plot of q_t versus $t^{0.5}$. The Weber–Morris kinetic model data were divided into two sections, and the Weber–Morris kinetic model-related constants are summarised in Table 1.

The linear plots of $(-\ln(1 - F) - 0.4977)$ versus t at different temperatures were obtained, and the related parameters were calculated. The results indicated that the

Table 1 Parameters of Weber–Morris intraparticle diffusion model for Eu(III) adsorption on natural bamboo fibre (C is the intercept, K_e is the intraparticle diffusion rate constant, and R^2 is the linear correlation coefficient)

T (K)	Initial linear area			Second linear area		
	K_{e1} (kg/(mg $h^{0.5}$))	C_1	R_1^2	K_{e2} (kg/(mg $h^{0.5}$))	C_2	R_2^2
298	0.019	5.31	0.981	0.004	5.36	0.929
308	0.020	5.31	0.932	0.003	5.37	0.967
323	0.021	5.30	0.992	0.010	5.33	0.973

linear plots did not pass through the origin. This suggested that diffusion was an important control step and was involved in the adsorption process. Moreover, intraparticle diffusion could be divided into two stages: the initial stage of the curve and the buffering or equilibrium stage. The two stages fitted the experimental data well, which suggested that the intraparticle diffusion step was not the only control step, but it was one of the stages of the adsorption process.

3.5 Adsorption isotherms

The fitting curves of the adsorption of Eu(III) on NBFs at 298, 308, and 323 K were obtained and analysed. The Langmuir adsorption model could be described as follows [34]:

$$c_s = \frac{bc_{smax}c_e}{1 + bc_e}, \tag{18}$$

$$\frac{c_e}{c_s} = \frac{1}{bc_{smax}} + \frac{c_e}{c_{smax}}, \tag{19}$$

where c_{smax} is the maximum equilibrium adsorption capacity (mol/g), c_s is the Eu(III) concentration in the solid phase (mol/g), c_e is the Eu(III) concentration in the liquid phase (mol/l), and b (L/mol) is an adsorption temperature-related constant. According to Eq. (19), b and c_{smax} could be determined from intercept and slope, respectively, of the c_s versus c_e graph. The linear correlation coefficients of the Langmuir adsorption model were 0.963, 0.925, and 0.969, and the c_{smax} values were 1.09×10^{-4}, 9.71×10^{-4}, and 1.12×10^{-4} mol/g (16.57, 147.6, and 17.02 mg/g), at 298, 308, and 323 K, respectively. The adsorption capacity of NBFs for radionuclides is similar to those of other natural or modified biological adsorbents; however, the cost of NBFs is considerably lower than those of the other adsorbents [35]. Generally, the cost of NBFs is a fraction of that of other biological adsorbents and approximately 1% of the cost of synthetic functional materials.

As the temperature increased, the adsorption isotherm positions of Langmuir isotherm decreased, and the c_e/c_s values also decreased. This dynamic indicated that Eu(III) was distributed more in the solid phase than in the liquid phase at high temperatures and that high temperature could improve the adsorption process. In addition, as c_s increased, the Langmuir adsorption isotherms also presented an increasing trend, and the c_e/c_s values increased as well, which indicated that the increase in c_e could reduce the increase rate of c_s. Because the number of adsorption sites on the adsorbent surface was finite, the extra radionuclides would transfer from the solid phase to the liquid phase. For a certain concentration range, the fitting curve at high temperature (323 K) intersected the fitting curve at intermediate temperature (308 K), which indicated that radionuclides that were combined with organic matter of NBFs could desorb from the adsorbent surface at higher temperature and migrate from the solid phase to the liquid phase.

Moreover, the highest and lowest fitting curve temperatures of the Freundlich adsorption isotherms were 323 and 298 K, respectively. These results suggested that in the range of 298–323 K, high temperature was conducive to the adsorption of Eu(III) on NBFs.

According to the Freundlich isotherm model:

$$c_s = ac_e^n, \tag{20}$$

and its linear form could be written as follows:

$$\lg c_s = \lg a + \lg c_e, \tag{21}$$

where a (mol^{1-n} g^{-1} L^n) is the equilibrium concentration of adsorbent ions when $n = 1$, and n is the dependence of the adsorption on the equilibrium concentrations.

The R^2 values of the Freundlich adsorption model: 0.979, 0.960, and 0.986 at 298, 308, and 323 K, respectively, were close to 1. This suggested that the Freundlich adsorption model was more suitable for describing the Eu(III) adsorption behaviour on NBFs than the Langmuir adsorption model.

According to the above-mentioned experimental data, the instantaneous adsorption capacity of NBFs for Eu(III) was 5.382 mg/g, and the maximum adsorption capacity was 16.63 mg/g at 298 K. This adsorption capacity was relatively mediocre compared with that of other adsorbents and was significantly lower than those of bentonite and metal–organic framework materials [36, 37].

Using experimental data, the thermodynamic functions of the Eu(III) adsorption on NBFs could be calculated using the following equations:

$$\ln K = \frac{-\Delta H^0}{R} \times \frac{1}{T} + \frac{\Delta S^0}{R}, \quad (22)$$

and

$$\Delta G^0 = \Delta H^0 - T\Delta S^0, \quad (23)$$

where K is the adsorption equilibrium constant at different temperatures, and ΔH^0, ΔS^0, and ΔG^0 are the standard enthalpy, entropy, and Gibbs free energy changes, respectively. The values of $\ln K$ were obtained by plotting $\ln K_d$ versus c_e and extrapolating c_e to 0. The values of ΔH^0 and ΔS^0 were calculated from the slopes and intercepts of the $\ln K$ versus $1/T$ plots. The results indicated that ΔH^0 at 298, 308, and 323 K were positive (4.57 kJ/mol), which suggested that the adsorption reaction was an endothermic process. This also suggested that in the temperature range of 25–50 °C (298–323 K), Eu(III) was soluble in water and the hydration of the outer NBF sheath was destroyed before Eu(III) was adsorbed on it, which explained why this process required energy. The amount of required energy exceeded the quantity of heat released from the cation adsorption on the adsorbent surface. This theory demonstrated that the amount of heat absorbed during the desolvation process was higher than the adsorption heat within a certain range. At high temperatures, cationic desolvation occurred easier and therefore Eu(III) was more easily adsorbed [38]. Under the experimental conditions in this study, the adsorption reaction was a spontaneous process because ΔG^0 was negative (− 25.21, − 26.21, and − 27.71 kJ/mol, at 298, 308, and 323 K, respectively). As the temperature increased, the absolute value of ΔG^0 increased gradually, which indicated that temperature could accelerate the adsorption reactions. The ΔS^0 values of the adsorption process were positive and thus demonstrated that NBF adsorption was a spontaneous process.

4 Conclusion

In this study, NBF samples were prepared and characterised, and the application of NBFs for the removal of Eu(III) from aqueous solutions was studied using batch techniques. The main adsorption sites of NBFs were organic functional groups, and temperature could affect the combination of functional groups and NBF surface properties. Moreover, the pH value determined the hydrolysis of the organic functional groups, which affected the adsorption behaviour and adsorption performance of the NBFs. Furthermore, HA could improve Eu(III) adsorption on NBFs at low pH values and could inhibit its adsorption at high pH values. Cation exchange, outer-, and inner-sphere complexation were the main mechanism of the adsorption process in different pH ranges. The time required to achieve adsorption–desorption equilibrium was approximately 15 h, and the reaction could be described using the pseudo-second-order kinetic model. The maximum adsorption capacity was calculated to be 147.6 mg/g at 308 K. The Freundlich adsorption model fitted well the adsorption isotherms. Therefore, NBFs were determined to be an efficient, inexpensive, and easily available material for Eu(III)remediation from aqueous solutions.

References

1. L. Chen, X.J. Yu, Z.D. Zhao, Effect of humic acid, pH and ionic strength on the sorption of Eu(III) on red earth and its solid component. J. Radioanal. Nucl. Chem. **274**, 187–193 (2007). https://doi.org/10.1007/s10967-006-6814-0
2. B. Ivanova, M. Spiteller, Adsorption of uranium composites onto saltrock oxides-experimental and theoretical study. J. Environ. Radioactiv. **135**, 75–83 (2014). https://doi.org/10.1016/j.jenvrad.2014.03.019
3. X.X. Wang, Y.B. Sun, A. Alsaedi et al., Interaction mechanism of Eu(III) with MX-80 bentonite studied by batch, TRLFS and kinetic desorption techniques. Chem. Eng. J. **264**, 570–576 (2015). https://doi.org/10.1016/j.cej.2014.11.136
4. K. Cheng, Y.F. Zhu, W.J. Weng et al., Biocompatible Eu-doped TiO_2 nanodot film with in situ protein adsorption characterization property. Thin Solid Films **584**, 9–12 (2015). https://doi.org/10.1016/j.tsf.2015.01.003
5. H.N. Tran, S.J. You, A. Hosseini-Bandegharaei et al., Mistakes and inconsistencies regarding adsorption of contaminants from aqueous solutions: a critical review. Water Res. **120**, 88–116 (2017). https://doi.org/10.1016/j.watres.2017.04.014
6. Y. Xie, C.L. Chen, X.M. Ren et al., Emerging natural and tailored materials for uranium-contaminated water treatment and environmental remediation. Prog. Mater. Sci. **103**, 180–234 (2019). https://doi.org/10.1016/j.pmatsci.2019.01.005
7. Y.H. Wu, H.W. Pang, Y. Liu et al., Environmental remediation of heavy metal ions by novel-nanomaterials: a review. Environ. Pollut. **246**, 608–620 (2019). https://doi.org/10.1016/j.envpol.2018.12.076
8. Y. Xie, D.D. Shao, X.R. Lu et al., Spectroscopic investigation of enhanced adsorption of U(VI) and Eu(III) on magnetic attapulgite in binary system. Ind. Eng. Chem. Res. **57**, 7533–7543 (2018). https://doi.org/10.1021/acs.iecr.8b01803
9. W.B. Yang, J. Li, Y.X. Liu, Study on plant fiber/plastic composites as the substrate of floorboard. J. For. Res. **16**, 245–246 (2005). https://doi.org/10.1007/bf02856825
10. J.T. Wang, Y. Zheng, A.Q. Wang, Preparation and properties of kapok fiber enhanced oil sorption resins by suspended emulsion polymerization. J. Appl. Polym. Sci. **127**, 2184–2191 (2013). https://doi.org/10.1002/app.37783
11. Z.H. Li, M. Kobayashi, Plantation future of bamboo in China. J. For. Res. **15**, 233–242 (2004). https://doi.org/10.1007/BF02911032
12. L. Nayak, S.P. Mishra, Prospect of bamboo as a renewable textile fiber, historical overview, labeling, controversies and regulation. Fash. Text. **3**, 2–24 (2016). https://doi.org/10.1186/s40691-015-0054-5

13. M.F. Hamza, J.C. Roux, E. Guibal, Uranium and europium sorption on amidoxime-functionalized magnetic chitosan microparticles. Chem. Eng. J. **344**, 124–137 (2018). https://doi.org/10.1016/j.cej.2018.03.029
14. K.R. Zhu, C.L. Chen, J. Li et al., Alkali-treated cellulose fibers for U(VI) separation and enrichment. J. Radioanal. Nucl. Chem. **308**, 981–990 (2016). https://doi.org/10.1007/s10967-015-4527-1
15. A.N. Veleshko, S.A. Kulyukhin, I.E. Veleshko et al., Sorption of radionuclides from solutions with composite materials based on Mikoton natural biopolymer. Radiochemistry **50**, 508–514 (2008). https://doi.org/10.1134/S1066362208050135
16. W.M. Dong, X.K. Wang, J.Z. Du et al., Sorption and desorption characteristics of Eu(III) on red earth. J. Radioanal. Nucl. Chem. **242**, 793–797 (1999). https://doi.org/10.1007/BF02347397
17. R.X. Cheng, Q.S. Zhang, S.J. Sui, Improvement of softening treatment technology of bamboo. Wood Sci. Technol. **40**, 327–335 (2006). https://doi.org/10.1007/s00226-005-0034-9
18. Y.Z. Xu, L.M. Yang, Z. Xu et al., Distinguishing malignant from normal stomach tissues and its in vivo, in situ measurement in operating process using FTIR Fiber-Optic techniques. Sci. China Ser. B: Chem. **48**, 167–175 (2005). https://doi.org/10.1360/04yb0135
19. K. Štamberg, P. BeneŠ, J. Mizera et al., Radiotracer study of the kinetics of complexation and decomplexation of Eu(III) with humic acid using ion exchange. J. Radioanal. Nucl. Chem. **258**, 347–360 (2003). https://doi.org/10.1023/A:1026246006953
20. T. Yu, S.M. Liang, T. Pan et al., Sorption kinetic studies of U(VI) on inorganic and organic modified red earth: comparison of linear and non-linear methods. J. Radioanal. Nucl. Chem. **314**, 297–305 (2017). https://doi.org/10.1007/s10967-017-5343-6
21. Z.Y. Zha, D.N. Wang, W. Hong et al., Influence of Europium speciation on its accumulation in *Brassica napus* and over-expressing BnTR1 lines. J. Radioanal. Nucl. Chem. **301**, 257–262 (2014). https://doi.org/10.1007/s10967-014-3120-3
22. Z.Y. Chen, Q. Jin, Z.J. Guo et al., Surface complexation modeling of Eu(III) and phosphate on Na-bentonite: binary and ternary adsorption systems. Chem. Eng. J. **256**, 61–68 (2014). https://doi.org/10.1016/j.cej.2014.06.096
23. N. Janot, P.E. Reiller, M.F. Benedetti, Modelling Eu(III) speciation in a Eu(III)/PAHA/α-Al_2O_3 ternary system. Colloid. Surf. A Physicochem. Eng. Asp. **435**, 9–15 (2013). https://doi.org/10.1016/j.colsurfa.2013.02.052
24. S. Barnie, J. Zhang, H. Wang et al., The influence of pH, coexisting ions, ionic strength, and temperature on the adsorption and reduction of hexavalent chromium by undissolved humic acid. Chemosphere **212**, 209–218 (2018). https://doi.org/10.1016/j.chemosphere.2018.08.067
25. Z.J. Guo, J. Xu, K.L. Shi et al., Eu(III) adsorption/desorption on Na-bentonite: experimental and modeling studies. Colloids Surf. A Physicochem. Eng. Asp. **339**, 126–133 (2009). https://doi.org/10.1016/j.colsurfa.2009.02.007
26. S.Y. Huang, H.W. Pang, L. Li et al., Unexpected ultrafast and high adsorption of U(VI) and Eu(III) from solution using porous Al_2O_3 microspheres derived from MIL-53. Chem. Eng. J. **353**, 157–166 (2018). https://doi.org/10.1016/j.cej.2018.07.129
27. Z.L. Niu, T. Ohnuki, E. Simoni et al., Effects of dissolved and fixed humic acid on Eu(III)/Yb(III) adsorption on aluminum hydroxide: a batch and spectroscopic study. Chem. Eng. J. **351**, 203–209 (2018). https://doi.org/10.1016/j.cej.2018.06.034
28. K. Vadivelan, K. Vasanth, Equilibrium, kinetics, mechanism, and process design for the sorption of methylene blue onto rice husk. J. Colloid Interface Sci. **286**, 90–100 (2005). https://doi.org/10.1016/j.jcis.2005.01.007
29. A. Baraka, Investigation of temperature effect on surface-interaction and diffusion of aqueous-solution/porous-solid adsorption systems using diffusion–binding model. J. Environ. Chem. Eng. **3**, 129–139 (2015). https://doi.org/10.1016/j.jece.2014.11.001
30. C.C. Yao, T.J. Chen, A new simplified method for estimating film mass transfer and surface diffusion coefficients from batch adsorption kinetic data. Chem. Eng. J. **265**, 93–99 (2015). https://doi.org/10.1016/j.cej.2014.12.005
31. S. Song, S. Zhang, S.Y. Huang et al., A novel multi-shelled Fe_3O_4@MnO_x hollow microspheres for immobilizing U(VI) and Eu(III). Chem. Eng. J. **355**, 697–709 (2019). https://doi.org/10.1016/j.cej.2018.08.205
32. Y.Z. Hu, C.F. Zhao, L. Yin et al., Combining batch technique with theoretical calculation studies to analyze the highly efficient enrichment of U(VI) and Eu(III) on magnetic MnFe2O4 nanocubes. Chem. Eng. J. **349**, 347–357 (2018). https://doi.org/10.1016/j.cej.2018.05.070
33. R. Jain, D. Dominic, N. Jordan et al., Higher Cd adsorption on biogenic elemental selenium nanoparticles. Environ. Chem. Lett. **14**, 381–386 (2016). https://doi.org/10.1007/s10311-016-0560-8
34. P. Li, Q.H. Fan, D.Q. Pan et al., Effects of pH, ionic strength, temperature and humic acid on Eu(III) sorption onto iron oxides. J. Radioanal. Nucl. Chem. **289**, 757–764 (2011). https://doi.org/10.1007/s10967-011-1153-4
35. A.A. Tolba, S.I. Mohamady, S.S. Hussin et al., Synthesis and characterization of poly(carboxymethyl)-cellulose for enhanced La(III) sorption. Carbohyd. Polym. **157**, 1809–1820 (2017). https://doi.org/10.1016/j.carbpol.2016.11.064
36. X.X. Wang, S.S. Lu, L. Chen et al., Efficient removal of Eu(III) from aqueous solutions using super-adsorbent of bentonite–polyacrylamide composites. J. Radioanal. Nucl. Chem. **306**, 497–505 (2015). https://doi.org/10.1007/s10967-015-4115-4
37. J. Li, X.X. Wang, G.X. Zhao et al., Metal–organic framework-based materials: superior adsorbents for the capture of toxic and radioactive metal ions. Chem. Soc. Rev. **47**, 2322–2356 (2018). https://doi.org/10.1039/c7cs00543a
38. Q.H. Fan, D.D. Shao, Y. Yu et al., Effect of pH, ionic strength, temperature and humic substances on the sorption of Ni(II) to Na-attapulgite. Chem. Eng. J. **150**, 188–195 (2009). https://doi.org/10.1016/j.cej.2008.12.024